

FlowTouch: View-Invariant Visuo-Tactile Prediction

Seongjin Bien^{*1}, Carlo Kneissl^{*2}, Tobias Jülg^{*1}, Frank Fundel², Thomas Ressler-Antal², Florian Walter^{1,3}, Björn Ommer², Gitta Kutyniok² and Wolfram Burgard¹

Abstract—Tactile sensation is essential for contact-rich manipulation tasks. It provides direct feedback on object geometry, surface properties, and interaction forces, enhancing perception and enabling fine-grained control. An inherent limitation of tactile sensors is that readings are available only when an object is touched. This precludes their use during planning and the initial execution phase of a task. Predicting tactile information from visual information can bridge this gap. A common approach is to learn a direct mapping from camera images to the output of vision-based tactile sensors. However, the resulting model will depend strongly on the specific setup and on how well the camera can capture the area where an object is touched. In this work, we introduce FlowTouch, a novel model for view-invariant visuo-tactile prediction. Our key idea is to use an object’s local 3D mesh to encode rich information for predicting tactile patterns while abstracting away from scene-dependent details. FlowTouch integrates scene reconstruction and Flow Matching-based models for image generation. Our results show that FlowTouch is able to bridge the sim-to-real gap and generalize to new sensor instances. We further show that the resulting tactile images can be used for downstream grasp stability prediction. Our code, datasets and videos are available at <https://flowtouch.github.io>

I. INTRODUCTION

The sense of touch helps us interact with the world in our everyday lives. Imbuing robots with similar capabilities has been a longstanding goal in the field. Many works in this domain have been accelerated in recent years thanks to the introduction of low-cost visuo-tactile sensors such as GelSight [1] and DIGIT [2], and the rapid advancement of vision processing techniques that complement these sensors. Still, efficiently integrating information from these sensors to boost robot performance remains an active field of research.

It has been shown that tactile data provides meaningful signals to improve the performance of complex manipulation tasks [3], [4], [5], [6], as they provide fine-grained information about the interaction that is not directly observable through vision alone. However, tactile sensors only provide relevant output during physical contact. As a result, at the beginning of a manipulation task, robots must rely primarily on vision to perceive and reason about their environment. To effectively integrate these complementary modalities, a robot should anticipate the expected tactile feedback before contact, reflecting the close alignment of vision and touch observed in the brain [7], [8]. Such a prediction enables more

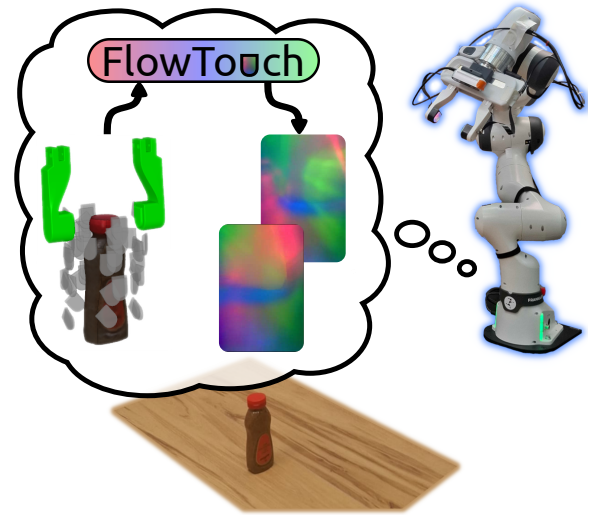


Fig. 1. FlowTouch at a glance: The robot first looks at the object and creates a mesh with scene mesh generation foundation models. Given the particular touch point on the mesh and the static background image of the tactile sensor, FlowTouch then predicts the resulting tactile image.

informed action planning and smoother transitions from non-contact to contact interaction.

Several works have explored this direction by leveraging recent advances in deep learning-based visual processing to train generative models that predict tactile sensor outputs conditioned on camera images [9], [10], [11]. However, learning a direct mapping from camera space to tactile space makes incorporating prior information difficult, requiring huge amounts of data across different scenes and objects to ensure good performance and generalization. Simulation can only partially mitigate this issue as both RGB renderings and tactile sensor models introduce a domain shift relative to real-world data. However, only a small fraction of visual features is relevant for tactile prediction, which mainly depends on geometric features. Including object-centric geometry information can therefore mitigate this issue by abstracting away from visual details not relevant for tactile sensing. However, this is difficult for purely vision-based end-to-end models.

In this work, we propose *FlowTouch*, a vision-to-touch framework that addresses this gap by explicitly leveraging geometric information to condition a Flow Matching-based generative model for predicting static tactile sensations from camera images. By lifting target objects from 2D observations into 3D representations using scene mesh generation foundation models, FlowTouch achieves increased robustness to viewpoint variations and scene-level changes.

*Equal contribution

¹Department of Computer Science & Artificial Intelligence, University of Technology Nuremberg, Germany. Contact: seongjin.bien@utn.de

²Ludwig Maximilian University of Munich

³TUM School of Computation, Information and Technology, Technical University of Munich, Germany

In summary, we make the following contributions:

- 1) We introduce a generative framework conditioned on geometry that predicts tactile signals without requiring exploratory robot motion beyond initialization.
- 2) We propose a simulation-to-real training method based on the mesh data of geometric primitives obtained via simulation and show that it improves output quality, substantially reducing the need for costly real-world data collection.
- 3) We demonstrate our framework’s capability by empirically verifying its strong generalization across scene variations and sensor instances, and its ability to generate relevant information for downstream manipulation tasks through grasp stability experiments.

II. RELATED WORK

A. Vision-to-Tactile Image Prediction

Previous work on robotic vision-to-tactile image prediction typically conditions a generative model on camera images captured during tactile interaction to produce the resulting visuo-tactile signal. Both VisGel [11] and ViTac-Gen [9] follow this approach, encoding interaction images and directly using the resulting representation. Because such conditioning inherently entangles scene and viewpoint with tactile-specific information, these methods often struggle to transfer beyond a benchmark setup. In contrast, ObjectFolder Benchmark [12] uses a pre-contact image from the same viewpoint as the target visuo-tactile observation, reframing the prediction as an inpainting task where much of the required geometric information is already present. Both paradigms require the robot to move close to the contact pose to acquire suitable inputs, which limits their practical use.

The closest parallel to our proposed work is Touching a NeRF [13], which trains a neural radiance field (NeRF) per object to render RGB and depth images from perspectives similar to the ObjectFolder Benchmark to be used as conditioning for a generative model. However, this approach requires object-specific training data for each novel instance, limiting its scalability. We address these issues directly by leveraging foundation models to lift objects from image to geometric space, thereby improving robustness to novel objects and scene variations, and motion-free input acquisition for tactile prediction.

B. Mesh-based Tactile Image Generation in Simulation

Visuo-tactile sensors such as GelSight [1] and DIGIT [2] capture the deformation of a silicon surface upon contact. Several sophisticated simulation methods have been introduced to enable the generation of tactile images at scale. TACTO [14] emulates contacts and renders tactile images using off-the-shelf rendering and simulation engines. Other approaches combine finite element methods with either rendering engine-based [15], [16] or data-driven methods [17], [18] to simulate both the tactile image and the deformation of the soft silicon pad to achieve higher fidelity. However, simulation data often suffer from non-trivial sim-to-real gap, preventing their direct application in real-world scenarios

without significant effort [19], [20]. Our model leverages simulation data generated for large-scale pretraining and uses learning-based adaptation on real data to narrow the sim-to-real gap, enabling more robust tactile image generation.

C. Tactile Datasets

Existing tactile datasets combine touch with visual observations and, in some cases, object geometry and pose supervision. ObjectFolder 1.0 [10] and 2.0 [21] provide a multimodal dataset comprising over 1000 objects in neural implicit representations, albeit with simulated tactile signals. The succeeding ObjectFolderReal [12] provides paired camera, tactile, and robot pose data for 100 real-world objects, while YCB-Slide [22] includes real and simulated DIGIT data with accurate sensor poses and ground-truth meshes. In contrast, Touch-and-Go [23] and Touch Vision Language [24] focus on visual–tactile pairing without precise pose or geometric supervision.

For our proposed approach, explicit geometry and sensor pose are crucial for localizing touch on object surfaces. Although ObjectFolderReal and YCB-Slide provide this information, they offer limited pose and contact diversity, with most surface points sampled only once. We, therefore, introduce a large-scale simulation data generation pipeline that systematically varies contact locations and relative sensor poses to complement existing datasets.

III. METHODOLOGY

A. Preliminaries

We address the problem of predicting a tactile sensor image $\mathbf{x} \in \mathbb{R}^{H \times W \times 3}$ based on a set of given contextual signals $\mathbf{c} = \{\mathbf{m}, \mathbf{b}\}$, where $\mathbf{m} \in \mathbb{R}^{N_{\text{pcn}} \times 6}$ is a point cloud of 3D positions and their respective normals (PCN) randomly sampled around the contact point on the mesh (with $N_{\text{pcn}} = 5000$ points) and $\mathbf{b} \in \mathbb{R}^{H \times W \times 3}$ is a background image from the same tactile sensor captured in the base state without any contact. We learn the conditional distribution $p(\mathbf{x} | \mathbf{c})$ via a latent Flow Matching objective [25] on the compressed representation of \mathbf{x} .

B. FlowTouch

Fig. 2 shows an overview of FlowTouch’s architecture. The method consists of two components: the image-to-PCN sampling pipeline, and the Flow Matching model that generates the tactile image conditioned on the input PCN.

1) *Sampling the PCN*: In order to sample the PCN around the desired contact points on the target object, we first create a mesh of the object that is aligned with the robot coordinate frame to properly position the contacts from the robot gripper’s desired poses. We employ SceneComplete [26] to achieve this. The framework takes in RGB-D images, the camera intrinsic matrix, and a language description of the target object. It then performs object segmentation and image inpainting before feeding the results into a 2D-to-3D model, whose output is scaled and aligned to the original depth image using a 6-D pose estimation model.

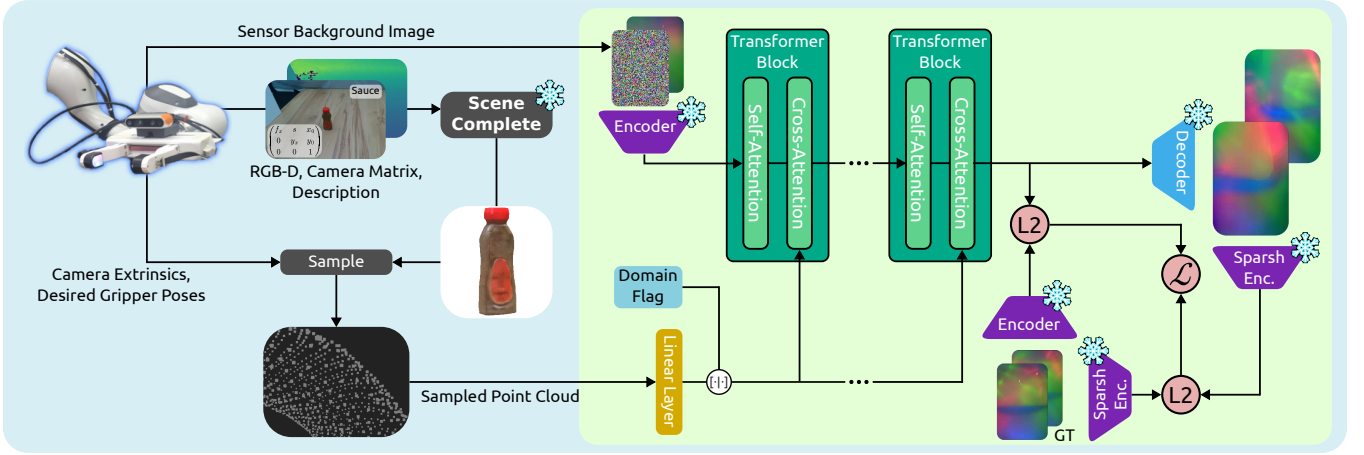


Fig. 2. The FlowTouch architecture: The blue area shows the image-to-PCN sampling pipeline, while the green area shows the generative model’s structure. Snowflakes indicate components with frozen weights.

With the aligned mesh, we can query the desired grasp pose and calculate the resulting poses of the tactile sensors mounted at the robot gripper’s fingertips. To ease the sampling process, we use MuJoCo [27] as follows: as MuJoCo creates a convex hull around a given collision-enabled geometry, we first decompose the output mesh into several convex submeshes using CoACD [28], and check for contacts only on those meshes, while keeping the original mesh for sampling. We then initialize a MuJoCo scene with the object mesh, its decomposed convex meshes, and the contact pad meshes of a pair of tactile sensors. To account for minor alignment errors, the contact pads are initialized at the gripper fingers’ open positions and adjusted along the gripper’s closing direction until both pads are penetrating any of the convex submeshes by 3 mm. Finally, we sample the PCN from the intersection of the mesh surface with the visualization areas of the two pads, which are smaller than the pads themselves. This PCN is used to condition the transformer-based image-to-image generative model.

2) *Latent Encoding*: Inspired by the success of Stable Diffusion [29], all image quantities are first compressed to a latent space using a frozen, tiny autoencoder [30] $\mathcal{E} : \mathbb{R}^{H \times W \times 3} \rightarrow \mathbb{R}^{(H/8) \times (W/8) \times 4}$, reducing spatial resolution by a factor of 8 and projecting to a 4-channel latent representation. We denote the latent encoding of the target tactile image as $\mathbf{z} = \mathcal{E}(\mathbf{x}) \in \mathbb{R}^{h \times w \times 4}$ and the decoder as \mathcal{D} .

3) *Flow Matching Objective*: We adopt the Conditional Flow Matching (CFM) framework [25] with a linear interpolant and define the forward process as a straight path from noise to data:

$$\mathbf{z}_t = (1 - t)\mathbf{z}_0 + t \cdot \mathbf{z}_1, \quad (1)$$

where $t \in [0, 1]$, $\mathbf{z}_0 \sim \mathcal{N}(\mathbf{0}, \mathbf{I})$ is a standard Gaussian random variable and \mathbf{z}_1 is a sample from the latent target distribution. A U-Net style Vision Transformer [31] denoted by $v_\theta(\mathbf{z}_t, t, \mathbf{m})$ is trained to regress the conditional velocity $u_t(\mathbf{z}_t | \mathbf{z}_1) = \mathbf{z}_1 - \mathbf{z}_0$ with the CFM objective

$$\mathcal{L}_{CFM}(\theta) = \mathbb{E}_{t, \mathbf{z}_0, \mathbf{z}_1} \left[|v_\theta(\mathbf{z}_t, t, \mathbf{m}) - (\mathbf{z}_1 - \mathbf{z}_0)|^2 \right]. \quad (2)$$

At inference time, the ordinary differential equation $\dot{\mathbf{z}}(t) = v_\theta(\mathbf{z}_t, t, \mathbf{m})$ is integrated from $t = 0$ to $t = 1$ using the Euler method with K uniform steps.

4) *Background Image as Channel-Stacked Context*: The background image \mathbf{b} encodes the sensor’s baseline appearance in the absence of contact and serves as a spatial prior. Its latent $\mathbf{b}_z = \mathcal{E}(\mathbf{b}) \in \mathbb{R}^{h \times w \times 4}$ is encoded once per sample and concatenated channel-wise with the noisy tactile latent:

$$\tilde{\mathbf{z}}_t = [\mathbf{z}_t | \mathbf{b}_z] \in \mathbb{R}^{h \times w \times 8} \quad (3)$$

We use $[\cdot | \cdot]$ to denote concatenation along the channel dimension. This formulation gives the backbone direct pixelwise access to the background at every integration step without additional cross-attention overhead, and preserves exact spatial registration between the deformation field and the sensor baseline.

5) *Cross-attention Mesh Conditioning*: The sampled PCN of shape $\mathbf{m} \in \mathbb{R}^{N_{\text{pcn}} \times 6}$ are linearly projected by $\mathbf{W}_{\text{mesh}} \in \mathbb{R}^{6 \times d_k}$ to form the cross-attention context $\mathbf{m}\mathbf{W}_{\text{mesh}}$ where $d_k = 768$ is the hidden dimension. In each transformer layer, the spatial tokens \mathbf{X} serve as queries while the mesh context provides keys and values, allowing every spatial location to attend over all N_{pcn} points. Thus, our attention block looks as follows:

$$\text{CrossAttn}(\text{SelfAttn}(\mathbf{X}), \mathbf{m}\mathbf{W}_{\text{mesh}}). \quad (4)$$

6) *Domain Adaptation*: In order to bridge the domain gap between simulated sensor values from our synthetic Taxim-generated dataset and datasets recorded with physical sensors, we employ a two-stage learning approach: First, we pretrain only on synthetic data for 30k steps with batch size 128. It is about 100 times larger than our real-world dataset and consists of different basic geometric shapes and our two sensor types, as detailed in Sec. III-C. Afterwards, we start a finetuning phase for another 20k steps where we mix in real data but only weigh it with 20%. The remaining 80% is still filled with synthetic data to avoid catastrophic forgetting. We refer to this strategy as *Naive Finetuning* and use it as our baseline to ablate further domain adaptation methods on top.

To help the model generalize to core concepts shared across domains, we also implemented a domain conditioning token, a standard technique for domain adaptation [32], [33]. We add a simple domain flag $dom \in \{0, 1\}$ (0 for synthetic and 1 for real) which is used to retrieve a learnable embedding $\mathbf{W}_{dom} \in \mathbb{R}^{d_k}$ and appended to the PCN information used in cross attention:

$$\text{CrossAttn}(\text{SelfAttn}(\mathbf{X}), [\mathbf{m}\mathbf{W}_{pcn}|\mathbf{W}_{dom}]) \quad (5)$$

This training technique is referred to as Domain Conditioning.

We also experiment with resetting the optimizer state and dropping its learning rate by a specified factor. This avoids updating the weights in the wrong direction with the AdamW momentum of the pretraining dataset when finetuning starts. We refer to this as Optimizer Reset.

Overfitting is a major challenge in domain adaptation when one domain has significantly less data, causing models to merely memorize the training set. To encourage generalization, we experiment with color augmentations (hue, saturation, brightness)—referred to as *Data Augmentation*—to artificially expand the dataset and mitigate this behavior.

The output of visuo-tactile sensors depends largely on the specific hardware used, and thus, two identical touches can yield completely different visual readings across different hardware. To mitigate this problem, we incorporate Sparsh [34], a self-supervised encoder for tactile predictions. It is able to produce compressed embeddings that retain most of the relevant information of the original tactile image, such as geometry, normal and shear forces, across a wide variety of sensor types. We hypothesize that a good tactile prediction from our model should be close to the ground truth in the Sparsh embedding space, as the embeddings retain information relevant to downstream tasks while ignoring less relevant data, such as sensor-specific noise. Thus, we include a loss objective to enforce that our predictions are consistent in the Sparsh embedding space.

More formally, let $\mathcal{E}_{\text{Sparsh}} : \mathbb{R}^{H \times W \times 3} \rightarrow \mathbb{R}^{h' \times w' \times 6}$ denote the static Sparsh encoder. In order to include this perception-based loss in our Flow Matching objective, we generate images with a single prediction from our Flow Matching model. For this, we reuse the \mathbf{z}_t computed for the Flow Matching loss and compute $\hat{\mathbf{z}}_1 = \mathbf{z}_t + (1 - t) \cdot v_\theta(\mathbf{z}_t, t, \mathbf{m})$. The Sparsh-based perceptual loss objective can then be formulated as

$$\mathcal{L}_{\text{Sparsh}} = \|\mathcal{E}_{\text{Sparsh}}(\mathcal{D}(\hat{\mathbf{z}}_1)) - \mathcal{E}_{\text{Sparsh}}(\mathbf{x}_1)\|_2, \quad (6)$$

where x_1 denotes the ground truth tactile image.

$$\mathcal{L}_{FT} = \mathcal{L}_{CFM} + \mathcal{L}_{\text{Sparsh}}. \quad (7)$$

We refer to this training technique as *Sparsh Perceptual Loss*.

C. Synthetic Data Generation

A major benefit of working directly in geometric space is the considerably reduced sim-to-real gap compared to image-based approaches. To fully leverage this advantage, we design a simulation data generation pipeline that captures

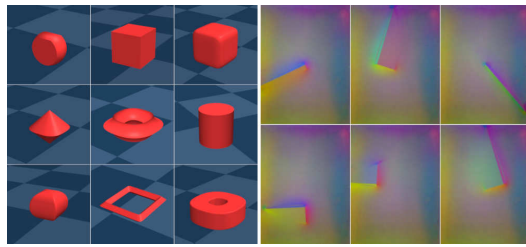


Fig. 3. *Left*: A selection of primitive geometries used for generating the simulation data. *Right*: Taxim GelSight images rendered from a single contact point (corner of a cube), with local translations and rotations.

a wide range of local surface geometries that visuo-tactile sensors may encounter in the wild.

We integrate Taxim [18] into MuJoCo [27], leveraging its parametrizable primitive geometries and built-in contact handling to generate diverse shapes efficiently. By varying geometric parameters, we can construct a large library of objects (Fig. 3, left) whose properties reflect those observed in existing tactile datasets and household items. Rather than sampling surfaces uniformly—which would over-represent flat regions—we explicitly select geometrically informative locations (e.g., edges and corners) to maintain a balanced coverage. At each location, we apply combinations of small local translations and rotations on the sensor to simulate realistic contact variations, and render the tactile image and sample the contact PCN (Fig. 3, right). This process produces over 100k unique samples in under an hour on a consumer-grade laptop (i9-13900HX), but could be substantially sped up through a GPU implementation.

Because PCNs sampled from such synthetic geometries are perfectly smooth, we inject multi-scale Gaussian noise along sampled normals to mimic reconstruction artifacts typical of learned mesh generation. Additionally, to reduce sensor-specific bias, we randomize the background image for each render.

IV. RESULTS

To verify whether our model is capable of generating visuo-tactile predictions, we evaluate it on a variety of datasets. We employ the ObjectFolderReal and YCB-Slide datasets for GelSight and DIGIT respectively. Both come with ground truth meshes for real objects, along with tactile images from their respective sensors as well as their sampling poses. This allows us to sample the PCNs required for our model. We preprocess the datasets to ensure that the tactile images line up with the poses on the meshes, filtering out those that deviate too much, and create a train/validation split on the object level. Additionally, we generate a large simulation dataset from 195 unique geometric primitives with the method described in Sec. III-C for both sensor types using the background images from those datasets along with our own digit sensors. The dataset details are shown in Tab. I under the names OFR-G, YCB-D, SIM-G and SIM-D respectively, and call the mix of these four Mixed-DG.

TABLE I
LIST OF DATASETS USED FOR EVALUATION. * INDICATES
WITHIN-OBJECT SPLIT.

Name	Sensor	Training # (# obj.)	Validation # (# obj.)
OFR-G	GelSight	887 (36)	135 (6)
SIM-G	GelSight	200K (135)	113K (60)
YCB-D	DIGIT	2578 (7)	1084 (3)
SIM-D	DIGIT	200K (135)	—
SELF-D	DIGIT	—	547 (13)
GS-G	GelSight	13372 (6*)	3379 (6*)

TABLE II
ABLATION STUDY ON NETWORK DESIGN CHOICES EVALUATED ON THE
GELSIGHT OFR DATASET. ALL METRICS ARE REPORTED ON THE
HELD-OUT VALIDATION SET.

Variant	PSNR (\uparrow)	SSIM (\uparrow)	LPIPS (\downarrow)
Base	24.28	0.52	0.40
BG-Enc	25.52	0.57	0.34
BG-Scene-Enc	24.91	0.54	0.38
BG-Stack	25.53	0.59	0.35

A. Model Architecture Design Choices

To validate different model design choices we train different FlowTouch variants on the OFR-G dataset and conduct an ablation study to assess the contribution of each individual design choice summarized in Tab. II. We refer to the vanilla FlowTouch model Base. BG-Stack refers to the extension of using the background stacking method as described in Sec. III-B.4. We compare BG-Stack to an alternative approach of using the DINOv2 [35] image encoder (referred to as BG-Enc) and condition our Flow Matching process on it during training. We also train a version that takes the DINOv2-encoded RGB image of the overall touch interaction scene as an additional input, called BG-Scene-Enc. Quantitative results on the validation set are reported in Tab. II using three image quality metrics: PSNR, SSIM, and LPIPS [36]. While PSNR and SSIM are standard reconstruction quality measures, they exhibit well-known limitations in the tactile domain, where signals are spatially sparse and sensitive to rotational and translational misalignment introduced by real-world calibration inaccuracies. LPIPS, as a learned perceptual metric, serves as a complementary measure that is more robust to such artifacts.

Overall, our PCN-based tactile prediction method achieves competitive performance across all metrics. The reported PSNR values are consistent with those by Gao *et al.* [12] on their visuo-tactile-cross-generation task, despite them having access to a larger training corpora and relying exclusively on simulation data.

Consistent with observations in prior work [11], we find that providing the model with an undeformed background tactile image as input yields measurable performance gains. All variants that make use of the background tactile (BG-Stack, BG-Enc, BG-Scene-Enc) outperform the unconditioned Base variant across all three metrics. Notably, aug-

menting the model with scene-level visual context does not yield to further improvement. Notably, BG-Scene-Enc underperforms BG-Enc across all metrics, suggesting that the scene embedding provides a weak signal that may interfere with tactile feature learning.

Finally, BG-Stack achieves performance on par with BG-Enc, while avoiding the additional parameters and inference cost of the DINOv2 encoder. We also evaluated the impact of using a pretrained PCN encoder (specifically, TripoSG’s [37] encoder), but found little evidence of it outperforming the simple linear layer in our design, possibly due to the relatively small number of the PCN input. Given this parity in performance, we adopt BG-Stack as our default configuration in all subsequent experiments.

B. Training Techniques for Domain Adaptation

We employed several domain adaptation techniques to bridge the sim-to-real gap in our data and to avoid catastrophic forgetting when fine-tuning on a much smaller real dataset as described in Sec. III-B.6. An ablation study of these training methods is shown in Tab. III on the same metrics as those used for the architecture study above. Our baseline (Naive Finetuning) is trained with the pretraining/fine-tuning approach outlined in Sec. III-B.6. All other methods use the baseline with only their specific technique added. The metrics are provided as differences towards the baseline and are given for three physical datasets: YCB-D, a DIGIT dataset which was part of fine-tuning; OFR-G, a GelSight dataset also part of fine-tuning; and SELF-D, our self collected DIGIT dataset not seen in training. All metrics are shown on the validation datasets.

Tab. III shows that Data Augmentation does not improve the training. Instead, it hurts all metrics compared to the baseline training. We hypothesize that its benefit of improving generalization does not apply here, as it obfuscates the color space which encodes important geometric data about the deformation. The Sparsh Perceptual Loss slightly hurts the GelSight performances but increases the PSNR values for both DIGIT datasets. This is expected as it optimizes in the Sparsh embedding space, which does not necessarily imply improving metrics computed in the RGB space. However, as we will later demonstrate, it can improve performance in downstream application and is therefore an important feature of our method.

The Optimizer Reset shows slightly better values especially for the PSNR of the DIGIT datasets. In this variant, the optimizer does not experience a sudden shock when it sees new data, leading to smoother learning phase transition and increased generalization. The Domain Conditioning significantly boosts performance across the board and is, thus, our best performing technique. This result was expected, as this technique helps the model to focus on the high-level similarities between the domains and lead to better generalization.

During training, we noticed that doubles edges are almost perfectly learned in our simulation-only pretraining phase across all configurations, thanks to a similar geometry being

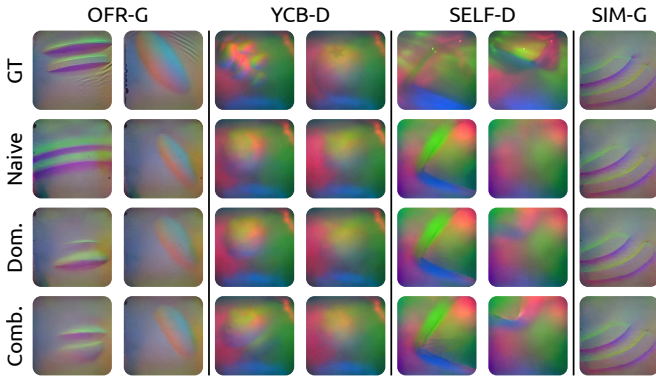


Fig. 4. Tactile predictions of the model ablations listed in Tab. III. Samples are taken from the validation dataset.

present in the simulation datasets. Once the fine-tuning starts, some of these properties are forgotten and relearned after some steps, however with decreased quality. Although Domain Conditioning was capable of retaining it better than others, we hypothesize these double edges have not been learned in generalized way, which is why they do not transfer well even under this condition. Additionally, injecting a similar multi-scale Gaussian noise to the ground truth PCNs as we do to the simulation-generated data improved the sim-to-real transfer.

Based on these results, we trained a final model which combines Sparse Perceptual Loss, Optimizer Reset and Domain Conditioning which we refer to as Combined. Interestingly, this variant scores slightly worse than the Domain Conditioning variant. However, based on the visualization of the prediction (such as OFR-G, left and SELF-D, right in Fig. 4), we hypothesize that the combined techniques helps to retain more tactile-relevant features in the image, at the cost of the pixel-based metrics.

C. Generalization Towards New Sensor Instances

To test our model’s ability to predict tactile images in a zero-shot manner, we collected our own dataset using the setup shown in Fig. 5 on 13 different common grocery and household objects. Our setup consists of a FR3 robot and gripper with a 3D-printed fingers for mounting the DIGIT sensors, and a wrist-mounted D435i camera, and use Robot Control Stack [38] for orchestrating the setup. After fixing the object onto the table, we take a scene picture for SceneComplete by moving the robot backwards, and generate the mesh as described in Sec. III-B.1. Afterwards, we put the robot in guiding mode to collect touch samples, 537 in total. Finally, we use the robot’s kinematics combined with a calibrated camera to reconstruct the touch poses around the mesh. This dataset is kept entirely for testing zero-shot generalization. For training our model, we used the YCB-D and SIM-D datasets described above.

Tab. III shows a consistent pattern for the analyzed features on the SELF-D dataset as in the previous section. Nonetheless, compared to the other DIGIT-based real world dataset YCB-D, the metrics on our dataset are considerably worse.



Fig. 5. *Left*: Objects used for data collection. *Center*: Robot setup. *Right*: Collected grasp poses aligned to generated mesh, with unique color for each finger pair.

Besides the obvious impact of zero-shot evaluation, we suspect that seeing a sensor instance during training allows the model to pick up on instance-specific quirks. Additionally, images DIGIT has noticeably more artifacts than GelSight, which may be another contributing factor. Despite what the metrics might suggest, our model is still able to generalize to some extent, as seen in Fig. 4. For example, the first column of the SELF-D dataset shows that the geometric shape of the touched object is roughly captured. The second column shows an interesting observation, as it demonstrates that our Combined model is able to provide a sharper contact image than the Domain Conditioning. On the other hand, the Naive Finetuning fails to display anything.

D. Grasp Stability

Finally, we evaluate whether our tactile predictions preserve sufficient information for downstream robotic manipulation tasks. Specifically, we adopt the grasp stability estimation task [12], in which a binary classifier predicts grasp success from a tactile image acquired at a candidate contact location.

We use the ObjectFolder pipeline [12] to collect the dataset, called GS-G, which performs simple grasps over variations on height, rotation and xy -offsets in PyBullet. A single tuple of RGB-D camera images and a Tactim image is collected at the moment of the grasp, and a corresponding success label is created at the end of each episode. We made minor modifications in the dataset collection script to calculate the required PCN data, change the background to a random sample from OFR-G, and collected 10,000 samples for 6 objects (see Fig. 6) from the benchmark. We balanced the dataset to consist of roughly equal number of grasping successes and failures similar to how Gao *et al.* [10] did and split the dataset in a within-objects fashion.

The dataset configurations we investigate are depicted in Tab. IV together with the success rates of the respective experiment variants. We first train the binary classifier on the ground truth tactile from the GS-G dataset to establish our



Fig. 6. Meshes used for the ObjectFolder Benchmark grasp stability test.

TABLE III

QUANTITATIVE COMPARISON OF DIFFERENT SIM-TO-REAL TRAINING TECHNIQUES ACROSS THE PRETRAINING SIM-G, FINETUNING OFR-G, AND UNSEEN SELF-D DATASETS. VALUES FOR EXPERIMENTAL METHODS ARE SHOWN AS ABSOLUTE DIFFERENCES RELATIVE TO THE NAIVE FINETUNING BASELINE AND ARE CALCULATED ON THE VALIDATION DATASET.

Training Method	YCB-D			OFR-G			SELF-D (unseen)		
	PSNR (\uparrow)	SSIM (\uparrow)	LPIPS (\downarrow)	PSNR (\uparrow)	SSIM (\uparrow)	LPIPS (\downarrow)	PSNR (\uparrow)	SSIM (\uparrow)	LPIPS (\downarrow)
Naive Finetuning	20.23	0.612	0.284	24.58	0.553	0.410	16.05	0.355	0.415
Data Augmentation	-0.56	-0.015	+0.013	-0.43	-0.031	+0.009	-0.37	-0.030	+0.004
Sparsh Perceptual Loss	-0.20	-0.006	+0.005	+0.17	-0.001	-0.006	+0.06	-0.000	-0.002
Optimizer Reset	-0.03	-0.001	+0.000	+0.28	-0.005	-0.004	+0.07	+0.001	-0.001
Domain Conditioning	+2.18	+0.058	-0.055	+0.90	+0.029	-0.045	+0.78	+0.032	-0.021
Combined	+1.77	+0.050	-0.047	+0.86	+0.025	-0.041	+0.23	+0.001	-0.003

TABLE IV

TRAINING DATASET ABLATIONS FOR GRASP STABILITY TASK. VALUES ARE AVERAGED OVER 100 TRAININGS.

Name	Pre-training ds.	Fine-tuning ds.	Accuracy (%)
GT	—	—	85.83
A	Full GS-G	—	86.06
B	SIM- $\{D,G\}$	Full GS-G	85.17
C	Mixed-DG	10% of GS-G	83.74
D	SIM- $\{D,G\}$	OFR-G, YCB-D	81.35
D, no Sparsh	SIM- $\{D,G\}$	OFR-G, YCB-D	78.59

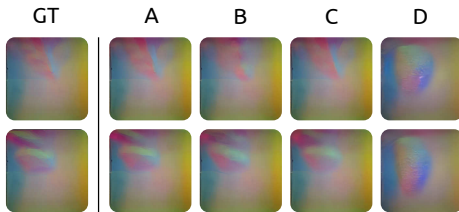


Fig. 7. Tactile predictions from the grasp stability task on the dataset ablations listed in Tab. IV. Samples are taken from the validation dataset. SELF-D has not been seen during training.

baseline variant, called GT, which serves as qualitative reference for our model’s capability. Variants A to C on the other hand are based on the predictions of our FlowTouch model in combination with the GS-G dataset. These experiments serve to validate the output quality of our framework and, at the same time, determine the effect of different training dataset regimes. Lastly, to evaluate our framework’s zero-shot capability in this context, we create variant D, which never sees any samples of the GS-G dataset during training. Visualizations of this experiment can be found in Fig. 7.

Notably, variant A manages to slightly exceed the baseline’s performance, while variant B comes very close to both of these results. We can see that variant C performs a bit worse, but still achieves a high accuracy at nearly 84%. This shows that the pretraining provides a model with strong priors that require little data to be finetuned and adapted to a new domain. Although variant D achieves the worst result as expected, its 81.35% accuracy indicates that our approach is capable of retaining important physical properties even across sensor types and domain gaps. Finally,

we ablated on variant D by training the model without Sparsh Perceptual Loss. This version only achieves 78.59% accuracy, supporting our hypothesis that the loss indeed enforces tactile information retention during training.

E. Limitations

Although the PCN-based tactile prediction framework shows promise, it has several limitations. First, its performance depends heavily on mesh quality. It is also highly sensitive to alignment in the robot frame, as PCN sampling requires millimeter-level accuracy that is often difficult to achieve in practice. However, ongoing advancements in mesh generation and pose estimation may mitigate these issues. While the model generalizes well to shapes represented in the training data, it struggles with unseen geometries. This limitation could be alleviated by scaling up the diversity and size of the simulated dataset. Finally, our model does not explicitly encode force and instead relies implicitly on the depth of the sampled PCN to render meshes at different forces. This could be remedied by pre-processing the input PCN on a nonlinear gel deformation equation, as suggested by TACTO [14].

V. CONCLUSION AND FUTURE WORK

In this work, we introduced FlowTouch, a vision-to-touch framework featuring a geometry-conditioned generative prediction model. By leveraging point clouds and their corresponding normals sampled from meshes, our framework is able to effectively abstract away from scene-specific information inherent in image-only methods, and benefits from simulation data to achieve good generalization across both novel object instances and sensor types. Furthermore, we show that FlowTouch’s output can be used to support downstream manipulation tasks even in zero-shot settings. Finally, our framework uses scene reconstruction methods to make real-world deployment feasible.

A promising direction for future work is to incorporate textures into the model’s conditioning. This will enable the prediction of high-resolution tactile features that are not captured by standard mesh generation or scanning methods, thereby making FlowTouch more widely applicable.

ACKNOWLEDGMENT

This work has been partially supported by the project GeniusRobot funded by the German Federal Ministry of Education and Research (BMBF grant no. 01IS24083). It also has been partially supported by the German Federal Ministry of Research, Technology and Space (BMFTR) under the Robotics Institute Germany (RIG). The authors acknowledge the HPC resources provided by the Erlangen National HPC Center (NHR@FAU) under the BayernKI project no. v106be.

REFERENCES

- [1] W. Yuan, S. Dong, and E. H. Adelson, “GelSight: High-resolution robot tactile sensors for estimating geometry and force,” *Sensors*, vol. 17, no. 12, 2017.
- [2] M. Lambeta, P.-W. Chou, S. Tian, B. Yang, B. Maloon *et al.*, “DIGIT: A novel design for a low-cost compact high-resolution tactile sensor with application to in-hand manipulation,” *IEEE Robotics and Automation Letters*, vol. 5, no. 3, 2020.
- [3] Y. Chen, M. Van der Merwe, A. Sipos, and N. Fazeli, “Visuotactile transformers for manipulation,” in *Proc. of the Conf. on Robot Learning (CoRL)*, 2023.
- [4] J. Hansen, F. Hogan, D. Rivkin, D. Meger, M. Jenkin, and G. Dudek, “Visuotactile-RL: Learning Multimodal Manipulation Policies with Deep Reinforcement Learning,” in *Proc. of the IEEE Int. Conf. on Robotics & Automation (ICRA)*, 2022.
- [5] C. Higuera, J. Ortiz, H. Qi, L. Pineda, B. Boots, and M. Mukadam, “Perceiving Extrinsic Contacts from Touch Improves Learning Insertion Policies,” <http://arxiv.org/abs/2309.16652>, 2023.
- [6] R. Calandra, A. Owens, M. Upadhyaya, W. Yuan, J. Lin *et al.*, “The feeling of success: Does touch sensing help predict grasp outcomes?” in *Proc. of the Conf. on Robot Learning (CoRL)*, 2017.
- [7] C. Keyzers, J. H. Kaas, and V. Gazzola, “Somatosensation in social perception,” *Nature Reviews Neuroscience*, vol. 11, no. 6, 2010.
- [8] N. Hedger, T. Naselaris, K. Kay, and T. Knapen, “Vicarious body maps bridge vision and touch in the human brain,” *Nature*, vol. 650, 2025.
- [9] Z. Wu, Y. Lin, Y. Zhao, X. Zhang, Z. Chen *et al.*, “ViTacGen: Robotic pushing with vision-to-touch generation,” *IEEE Robotics and Automation Letters*, vol. 10, no. 11, 2025.
- [10] R. Gao, Y.-Y. Chang, S. Mall, L. Fei-Fei, and J. Wu, “ObjectFolder: A dataset of objects with implicit visual, auditory, and tactile representations,” in *Proc. of the Conf. on Robot Learning (CoRL)*, 2021.
- [11] Y. Li, J.-Y. Zhu, R. Tedrake, and A. Torralba, “Connecting touch and vision via cross-modal prediction,” in *Proc. of the IEEE Computer Society Conference on Computer Vision and Pattern Recognition (CVPR)*, 2019.
- [12] R. Gao, Y. Dou, H. Li, T. Agarwal, J. Bohg *et al.*, “The Object Folder Benchmark: Multisensory learning with neural and real objects,” in *Proc. of the IEEE Computer Society Conference on Computer Vision and Pattern Recognition (CVPR)*, 2023.
- [13] S. Zhong, A. Albini, O. P. Jones, P. Maiolino, and I. Posner, “Touching a NeRF: Leveraging neural radiance fields for tactile sensory data generation,” in *Proc. of the Conf. on Robot Learning (CoRL)*, 2022.
- [14] S. Wang, M. Lambeta, P.-W. Chou, and R. Calandra, “TACTO: A fast, flexible, and open-source simulator for high-resolution vision-based tactile sensors,” *IEEE Robotics and Automation Letters*, 2022.
- [15] C. Zhang, S. Cui, J. Hu, T. Jiang, T. Zhang *et al.*, “TacFlex: Multi-mode tactile imprints simulation for visuotactile sensors with coating patterns,” *IEEE Transactions on Robotics*, 2025.
- [16] Z. Chen, S. Zhang, S. Luo, F. Sun, and B. Fang, “Tacchi: A pluggable and low computational cost elastomer deformation simulator for optical tactile sensors,” *IEEE Robotics and Automation Letters*, 2023.
- [17] Z. Si, G. Zhang, Q. Ben, B. Romero, Z. Xian *et al.*, “DIFFTACTILE: A physics-based differentiable tactile simulator for contact-rich robotic manipulation,” in *Proc. of the Int. Conf. on Learning Representations (ICLR)*, 2024.
- [18] Z. Si and W. Yuan, “Taxim: An example-based simulation model for gelsight tactile sensors,” *IEEE Robotics and Automation Letters*, vol. 7, no. 2, 2022.
- [19] W. Chen, Y. Xu, Z. Chen, P. Zeng, R. Dang *et al.*, “Bidirectional sim-to-real transfer for gelsight tactile sensors with cyclegan,” *IEEE Robotics and Automation Letters*, vol. 7, no. 3, 2022.
- [20] G. M. Caddeo, A. Maracani, P. D. Alfano, N. A. Piga, L. Rosasco, and L. Natale, “Sim2real bilevel adaptation for object surface classification using vision-based tactile sensors,” in *2024 IEEE International Conference on Robotics and Automation (ICRA)*, 2024.
- [21] R. Gao, Z. Si, Y.-Y. Chang, S. Clarke, J. Bohg *et al.*, “ObjectFolder 2.0: A multisensory object dataset for sim2real transfer,” in *Proc. of the IEEE Computer Society Conference on Computer Vision and Pattern Recognition (CVPR)*, 2022.
- [22] S. Suresh, Z. Si, S. Anderson, M. Kaess, and M. Mukadam, “Midas-Touch: Monte-Carlo inference over distributions across sliding touch,” in *Proc. of the Conf. on Robot Learning (CoRL)*, 2022.
- [23] F. Yang, C. Ma, J. Zhang, J. Zhu, W. Yuan, and A. Owens, “Touch and Go: Learning from human-collected vision and touch,” in *Advances in Neural Information Processing Systems*, 2022.
- [24] L. Fu, G. Datta, H. Huang, W. C.-H. Panitch, J. Drake *et al.*, “A touch, vision, and language dataset for multimodal alignment,” in *Proc. of the Int. Conf. on Machine Learning (ICML)*, 2024.
- [25] Y. Lipman, R. T. Q. Chen, H. Ben-Hamu, M. Nickel, and M. Le, “Flow matching for generative modeling,” in *Proc. of the Int. Conf. on Learning Representations (ICLR)*, 2022.
- [26] A. Agarwal, G. Singh, B. Sen, T. Lozano-Pérez, and L. P. Kaelbling, “SceneComplete: Open-world 3d scene completion in cluttered real world environments for robot manipulation,” *IEEE Robotics and Automation Letters*, vol. 11, no. 1, 2026.
- [27] E. Todorov, T. Erez, and Y. Tassa, “MuJoCo: A physics engine for model-based control,” in *Proc. of the IEEE/RSJ Int. Conf. on Intelligent Robots and Systems (IROS)*, 2012.
- [28] X. Wei, M. Liu, Z. Ling, and H. Su, “Approximate convex decomposition for 3d meshes with collision-aware concavity and tree search,” *ACM Transactions on Graphics*, vol. 41, no. 4, 2022.
- [29] R. Rombach, A. Blattmann, D. Lorenz, P. Esser, and B. Ommer, “High-resolution image synthesis with latent diffusion models,” in *Proc. of the IEEE Computer Society Conference on Computer Vision and Pattern Recognition (CVPR)*, 2022.
- [30] O. B. Bohan, “TAESD: Tiny autoencoder for stable diffusion,” <https://github.com/madebyollin/taesd>, 2023.
- [31] A. Dosovitskiy, L. Beyer, A. Kolesnikov, D. Weissenborn, X. Zhai *et al.*, “An image is worth 16x16 words: Transformers for image recognition at scale,” in *Proc. of the Int. Conf. on Learning Representations (ICLR)*, 2021.
- [32] H. Daumé III, “Frustratingly easy domain adaptation,” in *Annual Meeting of the Association of Computational Linguistics*, 2007.
- [33] M. Johnson, M. Schuster, Q. Le, M. Krikun, Y. Wu *et al.*, “Google’s multilingual neural machine translation system: Enabling zero-shot translation,” *Transactions of the Association for Computational Linguistics*, 2017.
- [34] C. Higuera, A. Sharma, C. K. Bodduluri, T. Fan, P. Lancaster *et al.*, “Sparsh: Self-supervised touch representations for vision-based tactile sensing,” in *Proc. of the Conf. on Robot Learning (CoRL)*, 2024.
- [35] M. Oquab, T. Darcet, T. Moutakanni, H. V. Vo, M. Szafraniec *et al.*, “DINOv2: Learning robust visual features without supervision,” *Transactions on Machine Learning Research*, 2024.
- [36] R. Zhang, P. Isola, A. A. Efros, E. Shechtman, and O. Wang, “The unreasonable effectiveness of deep features as a perceptual metric,” in *Proc. of the IEEE Computer Society Conference on Computer Vision and Pattern Recognition (CVPR)*, 2018.
- [37] Y. Li, Z.-X. Zou, Z. Liu, D. Wang, Y. Liang *et al.*, “Tripog: High-fidelity 3d shape synthesis using large-scale rectified flow models,” *IEEE Transactions on Pattern Analysis and Machine Intelligence*, 2025.
- [38] T. Jülg, P. Krack, S. Bien, Y. Blei, K. Gamal *et al.*, “Robot Control Stack: A lean ecosystem for robot learning at scale,” <https://arxiv.org/abs/2509.14932>, 2025.